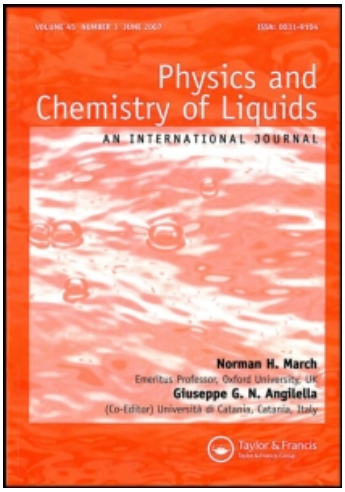

Physics and Chemistry of Liquids
Publication details, including instructions for authors and subscription information:
http://www.informaworld.com/smpp/title~content=t713646857

Transport properties of expanded rubidium: potential dependence

Raman Sharma[a]; K. Tankeshwar[b]
[a] Department of Physics, Himachal Pradesh University, Shimla - 171 005 India [b] Department of Physics, Panjab University, Chandigarh - 160 014 India

To cite this Article Sharma, Raman and Tankeshwar, K.(2006) 'Transport properties of expanded rubidium: potential dependence', Physics and Chemistry of Liquids, 44: 4, 387 — 399
To link to this Article: DOI: 10.1080/00319100600757201
URL: http://dx.doi.org/10.1080/00319100600757201

Physics and Chemistry of Liquids
Vol. 44, No. 4, August 2006, 387–399

Taylor & Francis
Taylor & Francis Group

Transport properties of expanded rubidium: potential dependence

RAMAN SHARMA*† and K. TANKESHWAR‡

†Department of Physics, Himachal Pradesh University,
Shimla – 171 005 India
‡Department of Physics, Panjab University,
Chandigarh – 160 014 India

(*Received 10 April 2006; in final form 12 April 2006*)

The effect of the potential shape on the transport properties of rubidium (Rb) metal along the liquid–vapor co-existence curve has been studied at six thermodynamic states by assuming that the particles of the system are interacting via the Lennard–Jones (LJ) potential with same effective size of the particle and well depth of the potential as that of the corresponding liquid–metal (LM) potential. Self-diffusion coefficient and coefficient of shear viscosity of expanded Rb have been calculated by using a simple model, which employs sum rules and provides a good description of transport coefficients both for LMs and LJ fluids. We have found that the sum rules are able to account for the observed differences in the behavior of velocity auto-correlation functions (VACFs) of LM and LJ fluids. The fact that the back scattering effects are more pronounced in LMs than in the case of LJ fluids can be understood in terms of enhanced values of frequency sum rules in case of harder potential. It is found that the normalized stress auto-correlation function decays much faster in harder potential than in liquid metal. The effect of the potential shape on the self-diffusion and the shear viscosity is found to decrease as one moves toward the critical point from near the triple point. The contribution due to three particle correlations is found to be more important in case of metals than in LJ fluids.

Keywords: Liquid rubidium; Lennard–Jones potential; Transport properties

1. Introduction

A deep understanding of the relationship between the properties of different liquids and the characteristics of the corresponding interaction potential is of great interest to set up a microscopic basis of the liquid state behavior. Therefore, it would be interesting to relate the most characteristic feature of the liquid metal (LM) and Lennard–Jones (LJ) potential to the different properties of the corresponding liquids. It has been found that the difference between the structure of these two kinds of liquids is quite

*Corresponding author. Email: sramanb70@lycos.com

Physics and Chemistry of Liquids
ISSN 0031-9104 print: ISSN 1029-0451 online © 2006 Taylor & Francis
DOI: 10.1080/00319100600757201

similar [1], while the dynamic properties of the LMs and rare gas liquids differ in some respect and are not completely understood. The difference in the dynamical properties of LMs and LJ fluids may be attributed to the softness of the potential core and to the differences in attractive forces [2,3]. Recently, Canales and Padro [3,4] studied the potential dependence of dynamical and transport properties of LMs and LJ fluids by choosing same effective particle size and well depth of LM potential of liquid Li near its triple point. It was observed that dynamical properties are strongly influenced by the softness of the potential core. However, this has been examined only near the triple point where the liquid is known to show the metallic character. Therefore, as one goes toward the critical point of metal, the differences in dynamical and transport properties of metals and that of inert fluids are not known yet. In the present work, we aim to study the effect of characteristic interaction potential on the transport properties of expanded Rb along the liquid–vapor co-existence curve. Along the liquid–vapour co-existence curve the region from intermediate temperature to critical point of Rb is of interest, as with the liquid/gas transition Rb undergoes a metal/non-metal transition [5]. Therefore, this region is of special interest to study the effect of softness of the potential core on dynamical properties of metal. Earlier molecular dynamics [6] and theoretical studies [7] have been carried out to study the static and transport properties of expanded Rb metal using pseudo potential theory.

To study the effect of potential as one goes toward the critical point of LM, in the present work, we assume that the particles of the system are interacting via the LJ potential whereas the parameters of potential, i.e., well depth and the first zero of the potential are same as that of the corresponding LM potential. The self-diffusion coefficient, D, and the coefficient of shear viscosity, η, of expanded Rb for six thermodynamic states have been calculated [7] by using the sum rules and a simple model [8,9]. This model makes use of the sum rules and had already provided a good description of the transport coefficients both for LMs [7,10,11] and LJ fluids [8,11,12]. The frequency sum rules of velocity and the transverse stress auto-correlation function have been studied to examine the effect of potential core on the time-dependent properties of the system. It is found that values of the frequency sum rules are higher for harder potential. The sum rules have been found to account for the observed differences in the behavior of velocity auto-correlation function (VACF) of Rb metal and corresponding LJ fluid. It is found that back scattering effects are more pronounced in case of LMs than in case of LJ fluids. It can be understood in terms of higher values of frequency sum rules in case of harder potential. The VACF of LM potential and that of the one corresponding to LJ potential are very similar near the critical point which is in contrast to the behavior near the melting point. On the other hand, the normalized transverse stress auto-correlation (TSAC) function decays much faster in LJ potential than in LM potential for all the thermodynamical states. The effect of potential shape on self-diffusion and shear viscosity is found to decrease as one moves toward the critical point from near the triple point. The contribution due to three particle correlations is found to be more effective in case of LMs than in case LJ fluids.

The article is organized as follows. Generalities are given in section 2, where we present a general framework for calculating the time correlation functions and transport coefficients. Difference in inter-atomic potential and radial distribution function of liquid Rb and LJ fluids under analogous conditions is also shown there.

Results and discussion are presented in section 3. Finally, conclusions are given in section 4.

2. Generalities

2.1. *Transport coefficients*

A transport coefficient κ can be expressed as a time integral of an appropriate auto-correlation function $C(t)$ as

$$\kappa = K \int_0^\infty C(t) \mathrm{d}t, \tag{1}$$

and is known as Green–Kubo formula [13]. Here, K is some thermodynamical quantity. The exact calculation of time correlation function (TCF), $C(t)$, is not feasible for the system of present interest as it amounts to finding out a solution of a many body problem. There exist a number of ways for the evaluation of $C(t)$ by using Mori's memory function formalism [13,14] and simplified description of atomic motion. However, in the present work, we make use of a model [8] which has provided good estimates for the coefficients of self-diffusion and shear viscosity of the LJ system [12] as well as for the LMs, especially expanded metals [7,15]. The expression for $C(t)$ in this model is given by

$$C(t) = C(0)\,\mathrm{sech}(t/\tau)\cos(\omega t). \tag{2}$$

In the above equation τ and ω are appropriate relaxations and frequencies, respectively. Using equation (2) in equation (1), we obtain an expression for a transport coefficient κ given as

$$\kappa = C_0 K \frac{\pi}{2} \tau\, \mathrm{sech}\left(\frac{\pi\omega\tau}{2}\right). \tag{3}$$

In order to calculate the self-diffusion coefficient and shear viscosity from the above expression we require values of parameters τ and ω. On comparing the short-time expansion of equation (2) with the exact short-time expansion of TCF, $C(t)$, we obtain

$$\tau^{-2} = \frac{C_4 C_0 - C_2^2}{4 C_2 C_0}, \tag{4}$$

and

$$\omega^2 = \frac{5C_2^2 - C_4 C_0}{4 C_2 C_0}, \tag{5}$$

where C_0, C_2, and C_4 are zeroth, second, and fourth frequency sum rules of TCF, $C(t)$. Expressions for these sum rules are available in literature [16,17] for velocity of

tagged particle and transverse stress correlation functions. It has been found that for some thermodynamic states of the system ω^2 become negative, whereas τ remains positive for the correlation of velocity of tagged particles. Under such circumstances, equations (2) and (3) can be rewritten as

$$C(t) = C(0)\,\mathrm{sech}(t/\tau)\cosh(\omega t), \tag{6}$$

and

$$\kappa = KC_0\frac{\pi}{2}\tau\sec\left(\frac{\pi\omega\tau}{2}\right). \tag{7}$$

In the present work we study the velocity and stress auto-correlation functions which are respectively, defined as

$$V(t) = \sum_{i=1}^{N}\frac{\langle\vec{v}_i(t).\vec{v}_i(0)\rangle}{\langle(\vec{v}_i)^2\rangle}, \tag{8}$$

and

$$S(t) = \langle J_{xy}(t)J_{xy}(0)\rangle, \tag{9}$$

where,

$$J_{xy}(t) = \sum_{i=1}^{N}[mv_{ix}(t)v_{iy}(t) + F_{iy}x_i(t)]. \tag{10}$$

In the equations above, x_i and $v_{ix}(t)$ are the x component of position and velocity of the ith particle at time t, respectively. F_{iy} is the y component of the force on the ith particle. K for VACF and TSAC function in equations (3) and (7) is k_BT/m and $1/Vk_BT$, respectively.

2.2. *Interatomic potential and radial distribution function*

In the present work, we assume that the particles of the system are interacting via the LJ potential

$$U(r) = 4\epsilon\left[\left(\frac{\sigma}{r}\right)^{12} - \left(\frac{\sigma}{r}\right)^{6}\right]. \tag{11}$$

The parameters of the potential, i.e., well depth (ϵ) and the effective particle size (σ) of the particles are kept the same as those corresponding to the LM potential used by Kahl and Kambayashi [6]. Values of the these parameters of the potential for different thermodynamical states are given in table 1. The comparison of LM potential and LJ potential is shown in figure 1 where we plot reduced potential, $U^*(r) = U(r)/\epsilon$ as a function of $r^* = r/\sigma$, for three of the thermodynamic states of Rb. The solid line

Table 1. Values of parameters of potential. T, ρ, σ, and ϵ represent temperature, mass density, the position of first zero, and well depth of LM potential respectively. $T^*(=k_B T/\epsilon)$ and $n^*(=\rho\sigma^3/m)$ represent reduced temperature and number density.

State	T (K)	ρ (gm cm^{-3})	σ (nm)	ϵ (10^{-12} ergs)	T^*	n^*
1	350	1.460	41.97862	0.07519852	0.6423	0.756
2	373	1.440	41.96285	0.07567248	0.68	0.745
3	1073	1.130	41.07260	0.08771005	1.60	0.55
4	1373	0.980	40.41258	0.09870986	1.92	0.45
5	1673	0.830	39.50153	0.1167129	1.97	0.36
6	1873	0.640	37.65076	0.1613590	1.60	0.24

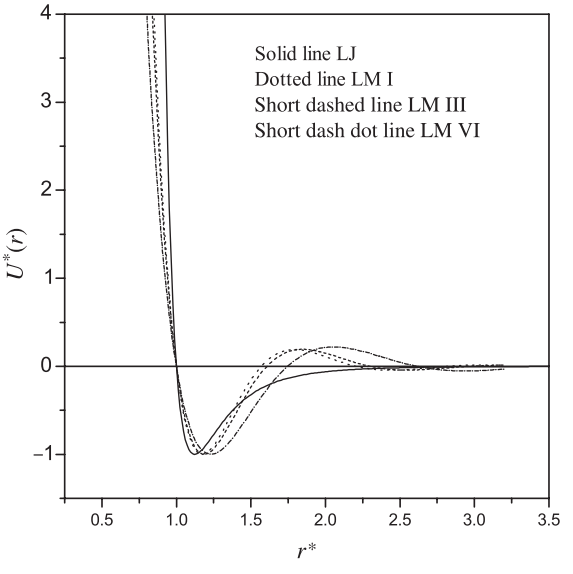

Figure 1. Reduced potential $U(r)/\epsilon$ as a function of r/σ. Solid line represents LJ potential, whereas dotted, dashed, dashed-dotted lines represent LM potential corresponding to 1st, 3rd, and 6th thermodynamic states, respectively.

represents LJ potential whereas dotted line, dashed line, and dashed-dotted line respectively, represent LM potential corresponding to 1st, 3rd, and 6th thermodynamic states. From figure 1, one can see that as one moves from 1st state near the melting point toward 6th state which is closer to critical point, LM potential becomes more shallower and position of the first minimum shifts toward larger r/σ. Another important quantity needed to evaluate is the radial distribution function, $g(r)$. In figure 2(a), (b), and (c) we compare radial distribution function $g(r)$ obtained for LJ potential using optimized cluster theory [18] with those obtained using LM potential [6] for 1st, 3rd, and 6th thermodynamic state, respectively. The solid line represents $g(r)$ of LJ potential whereas dotted lines correspond to LM potential. From the figure, it can be seen that first peak in $g(r)$, corresponding to LJ potential is sharper and at smaller value of r/σ than that corresponding to LM potential.

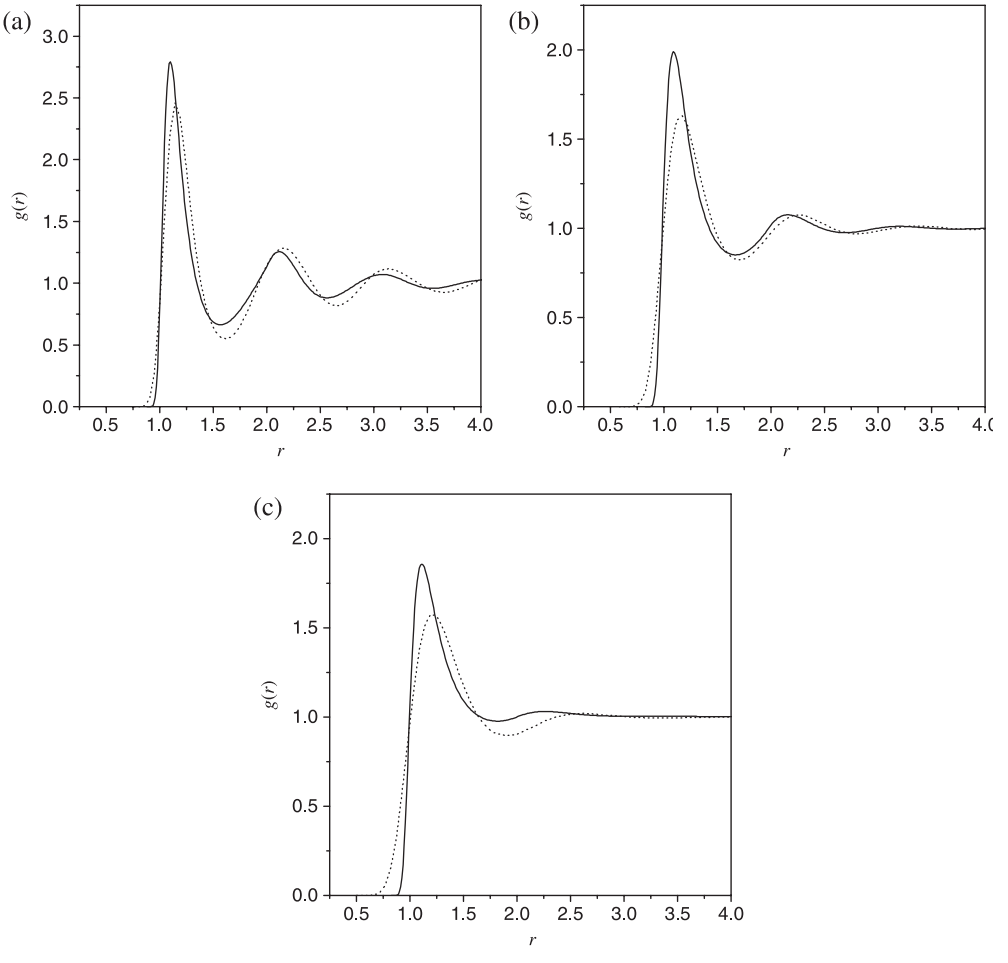

Figure 2. Static pair correlation function, $g(r)$, as a function of r/σ for (a) 1st thermodynamic state, (b) 2nd thermodynamic state, and (c) 6th thermodynamic state.

3. Results and discussion

3.1. *VAC function and self-diffusion*

The numerical results for the second and fourth sum rules of VAC function are obtained at six thermodynamic states of expanded Rb from the expressions already available in literature [9,11,16]. The main inputs required for this purpose are the interatomic potential and static correlation functions up to three particles. We use the LJ potential and the static pair-correlation function, $g(r)$, obtained by using optimized cluster theory of Sung and Chandler [18], discussed above. The triplet correlation function $g_3(\vec{r}_1, \vec{r}_2)$ involved in the fourth sum rules has been approximated using superposition approximation [19]. The numerical integration involved in the expressions of frequency sum rules is done by using Gauss-quadrature method. The accuracy of our numerical results for the sum rules is better than 5%. The numerical

Table 2. Values of second (V_2) and fourth (V_4) sum rules of the VAC. V_{mn} represents n body contribution to the mth sum rule.

	LJ potential			LM potential		
States	V_2 $(\epsilon/m\sigma^2)$	$V_{42} \times 10^{-2}$ $(\epsilon/m\sigma^2)^2$	$V_{43} \times 10^{-2}$ $(\epsilon/m\sigma^2)^2$	V_2 $(\epsilon/m\sigma^2)$	$V_{42} \times 10^{-2}$ $(\epsilon/m\sigma^2)^2$	$V_{43} \times 10^{-2}$ $(\epsilon/m\sigma^2)^2$
1	190.1242	1130.83	238.70	120.55	216.03	109.30
2	192.6315	1183.80	242.09	117.13	215.73	100.07
3	174.1056	1972.22	161.23	72.30	175.09	25.46
4	143.1741	1591.45	108.95	60.46	159.95	14.40
5	114.6221	1488.58	67.49	39.743	84.33	6.20
6	72.4896	965.25	26.86	23.884	38.279	1.85

Table 3. Values of relaxation time, $\tau(\sqrt{m\sigma^2/\epsilon})$ and vibrational frequency, $\omega(\sqrt{\epsilon/m\sigma^2})$ for VAC function.

	LJ potential		LM potential	
States	τ	ω	τ	ω
1	0.0868	7.587	0.164	9.123
2	0.0855	7.466	0.162	8.90
3	0.0617	9.418	0.140	4.586
4	0.0619	10.860	0.132	1.866
5	0.0567	14.00	0.146	2.70
6	0.0555	15.860	0.166	3.485

values of 2nd (V_2) and 4th (V_4) frequency sum rule of VAC function are given in table 2. The numerical values of these frequency sum rules obtained [7] by using corresponding LM potential are also given in table 2 for comparison. It is noted that for LJ potential, values of the sum rules are higher than those obtained by using LM potential. Since the major contribution to sum rules comes from small values of r, it implies that the softness of the potential reduces the contribution to the sum rules. Here, it may be recalled that up to 2nd and 3rd derivatives of the potential are involved in the expressions of second and fourth sum rules of VACF. From table 2 it can be seen that near the triple point the three body contribution to the 4th sum rules is 20% of the two body contribution whereas it is 50% in case of LM potential. Near the critical point the three body contribution reduces to 3% in LJ potential and 5% in LM potential. This shows that the contribution of higher-order correlations is more important in the case of a softer potential. It is also noted that $V_2(\mathrm{LJ})/V_2(\mathrm{LM})$ increases as one moves from 1st state to 6th state . This is as expected from the consideration of the potential and $g(r)$. However, it is more important to see the behavior of ω and τ which directly governs the time dependence of the VACF. The values of ω and τ are given in table 3. From table 3 one can see that the values of τ in the LJ potential are much smaller than the values corresponding to the LM potential. This in a cell picture implies that the metallic particles vibrate for longer time in a cell before it jumps to another cell. Near the melting point, the value of τ in the LJ potential differs from LM potential by about 50% and this difference increases as we go away from the triple point. At the critical point, this difference becomes 66%. On the other hand, it is found that ω^2 is negative in LJ potential for 3rd to 6th thermodynamic states whereas it is negative in LM potential for 5th and 6th thermodynamic states. It implies that

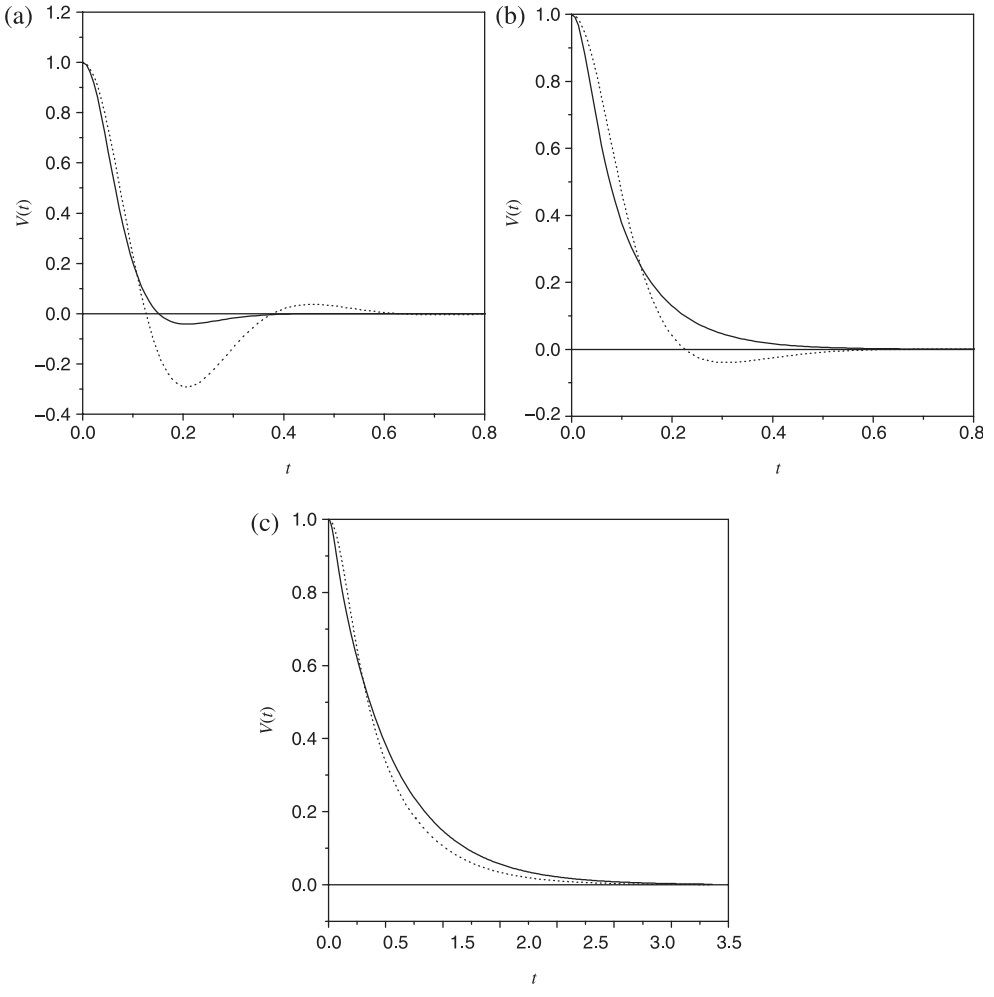

Figure 3. Velocity auto-correlation function, $V(t)$, *vs*. time in pico second for (a) 1st thermodynamic state, (b) 3rd thermodynamic state, and (c) 6th thermodynamic state.

back-scattering effects are more pronounced in case of LM than in case of LJ fluids. It is also noted that at thermodynamic states 1 and 2 where VACF, $V(t)$, is governed by same formula (equation (2)), the values of ω and $\omega\tau$ are higher in the case of the LM potential than in the case of the LJ potential, thus implying that $V(t)$ in the case of LM will have more oscillatory behavior than in the case of LJ fluids. This means that diffusive motion in LMs near melting point is closer to solid than in LJ fluids under analogous conditions. This is clearly seen from the normalized VACF $V(t)$ plotted in figure 3(a), (b), and (c) for the 1st, 3rd, and 6th thermodynamic states, respectively. Solid lines represent the results obtained using LJ potential whereas dotted lines represent results obtained using corresponding LM potential under analogous conditions. $V(t)$ for LM potential shows a deep minimum followed by oscillations while for LJ potential it shows only a shallower minimum.

The depth of the minimum goes on decreasing as we move away from the triple point toward the critical point. These findings for LJ and LM potential are already known and represent typical behavior of inert fluids and LMs. However, at the 5th (not shown) and 6th thermodynamic state, there is very little difference in the qualitative behavior of time evolution of $V(t)$. Thus, it is important to note that near the critical point $V(t)$ behaves in a similar fashion for LJ and LM systems, in spite of differences in potential and $g(r)$. The difference in the behavior of $V(t)$ near the melting point of Rb in our theoretical investigation can be attributed to smaller values of τ and ω in case of the LJ potential than that of LM. Since τ is directly proportional to Einstein frequency which is related to the second-order derivative of potential, we may thus attribute this behavior to the difference in the softness of the potential core.

Self-diffusion coefficients of the expanded Rb for six thermodynamic states have been calculated from equations (3) and (7). The calculated values of self-diffusion coefficient along with the earlier values [7] obtained using corresponding LM potential are given in table 4. The MD values [6] and experimental values [20] are also given there for comparison. Values of self-diffusion coefficient, D of LJ potential are higher than the the values obtained using LM potential. From table 4, it can be seen that there is a considerable difference in the values of D_{LJ} and D_{LM} near the melting point of LM, which is due to the fact that $\omega\tau$ is much larger in the case of LM potential than in the case of LJ fluids. This is in accordance with the earlier results [4], and this difference decreases as we go away from the melting point. The calculated values of diffusion coefficient for thermodynamic states 3rd to 6th, differ from the values obtained by using metallic potential at most by 12%.

3.2. *TSAC function and shear viscosity*

The numerical results of zeroth (S_0), second (S_2), and fourth (S_4) sum rules of TSAC function for six thermodynamic states of Rb are obtained using already known expressions [17]. The numerical values obtained for these sum rules using LJ potential and corresponding $g(r)$ are given in table 5. The values of these sum rules obtained [7] using LM potential are also given for comparison. The values of sum rules obtained using LJ potential are found to be higher than the values of sum rules using LM potential as has also been noted in the case of sum rules of VACF. Thus it

Table 4. Self-diffusion coefficients of expanded Rb for six thermodynamic states. D_{LJ}, D_{LM}, D_{MD}, and D_{expt} represent results obtained using LJ potential, LM potential, molecular dynamics and experimental results of Rb, respectively.

State	D_{LJ} ($\times 10^{-8}$ m^2 s^{-1})	D_{LM} ($\times 10^{-8}$ m^2 s^{-1})	D_{MD} ($\times 10^{-8}$ m^2 s^{-1})	D_{expt} ($\times 10^{-8}$ m^2 s^{-1})
1	0.532	0.302	0.298	0.352 ± 0.014
2	0.570	0.345	0.454	0.418 ± 0.020
3	2.72	2.421	3.429	3.661 ± 1.8
4	4.02	3.944	5.675	6.047 ± 4.4
5	6.27	6.279	8.483	9.346 ± 8.4
6	9.52	8.664	12.303	14.18 ± 14.7

Table 5. Values of zeroth (S_0), second (S_2) and fourth (S_4) sum rules of the TSAC function. S_{mn} represents n body contribution to mth sum rule.

	LJ potential					LM potential				
States	S_0 (ϵ^2)	S_{22} $\left(\times 10^{-2}\frac{\epsilon^3}{m\sigma^2}\right)$	S_{23} $\left(\times 10^{-2}\frac{\epsilon^3}{m\sigma^2}\right)$	S_{42} $\left(\times 10^{-4}\frac{\epsilon^4}{m^2\sigma^4}\right)$	S_{43} $\left(\times 10^{-4}\frac{\epsilon^4}{m^2\sigma^4}\right)$	S_0 (ϵ^2)	S_{22} $\left(\times 10^{-2}\frac{\epsilon^3}{m\sigma^2}\right)$	S_{23} $\left(\times 10^{-2}\frac{\epsilon^3}{m\sigma^2}\right)$	S_{42} $\left(\times 10^{-4}\frac{\epsilon^4}{m^2\sigma^4}\right)$	S_{43} $\left(\times 10^{-4}\frac{\epsilon^4}{m^2\sigma^4}\right)$
1	12.77	54.29	−19.36	865.50	−137.33	9.26	15.42	−9.90	45.97	−16.66
2	13.57	60.22	−20.63	1011.77	−153.44	9.55	16.11	−9.89	49.47	−16.78
3	28.56	214.83	−31.97	8423.84	−458.77	16.78	28.53	−7.71	156.03	−18.47
4	28.53	243.99	−23.69	11301.89	−392.39	16.95	29.96	−6.44	170.03	−19.12
5	21.89	188.06	−13.32	8974.33	−220.68	14.69	16.93	−2.75	89.96	−5.52
6	12.24	76.34	−4.05	2889.76	−53.47	8.01	7.44	−1.02	26.08	−1.43

is found that the values of the sum rules are larger for harder potential core. From table 5, one can also see that the ratio of three body contribution to the two body contribution to the second and fourth sum rules in LJ potential varies from 35 to 5% and 16 to 2%, respectively whereas in case of LM potential it varies from 64 to 14% and 35 to 5%. Thus, we can say that the contribution of higher-order correlation function is smaller in LJ fluids than in LMs.

The time evolution of TSAC function, $S(t)$, has been studied from equations (2) and (6). The normalized TSAC function $S(t)/S(0)$, for 1st, 3rd, and 6th thermodynamic states of Rb, is plotted in figure 4(a), (b) and (c), respectively. Solid lines represent results corresponding to LJ potential and the dotted lines represent results obtained using LM potential. It can be seen from figure 4(a)–(c) that $S(t)/S(0)$ decays faster in case of LJ potential than in case of the LM potential for all the thermodynamical states, thus implying that LM behaves more a viscous fluid than a fluid with a harder potential. Shear viscosity, η, of expanded Rb for six thermodynamic states has been calculated from equations (3) and (7). The calculated values of η along with earlier [7] values obtained using corresponding LM potential are given in table 6. Experimental [20] and MD [6] values of, η, are also given in table 6 for comparison. From table 6 it can be seen that the present values of η are smaller than the earlier values obtained using LM potential. This difference is found to be maximum near the triple point. The difference in the two viscosities decreases as one moves toward the critical point. However, unlike the diffusion coefficients, there remains a considerable difference in the time evolution of TSAC function and viscosities even near the critical point. This may be due to the fact that collective motion in liquids is more sensitive to the potential than the diffusive motion. Here, it may be recalled that values of the self-diffusion coefficients are larger in the case of fluids with harder potential. Thus one can say that fluids with a softer potential behave more a viscous fluid than that of a fluid with LJ potential under analogous condition. The difference between the values of η in some of the thermodynamic states is small as it appears from TSAC function. This is due to the fact that the shear viscosity is the area under the normalized TSAC function multiplied by zeroth sum rule S_0. Thus, we observe that the faster decay of $S(t)/S(0)$ is somewhat compensated by the larger value of shear modulus S_0 in the case of an LJ potential.

4. Summary and conclusion

The self-diffusion coefficient and shear viscosity of expanded Rb for six thermodynamic states have been studied along the liquid–vapor co-existence curve by considering that the particles of the system are interacting via LJ potential while the parameters of the potential, i.e., σ and ϵ are chosen as the same as those corresponding to a LM potential. The effect of the potential shape on velocity and TSAC function is studied by investigating the short-time properties of these time correlation functions. It is found that the values of the sum rules are higher for harder potential. Sum rules are found to account for the observed differences in the behavior of VACFs of metals and inert fluids. The fact that back scattering effects are more pronounced in LMs than in the case of LJ fluids can be understood in terms of an enhanced value of frequency sum rules in the case of a harder potential. It is found

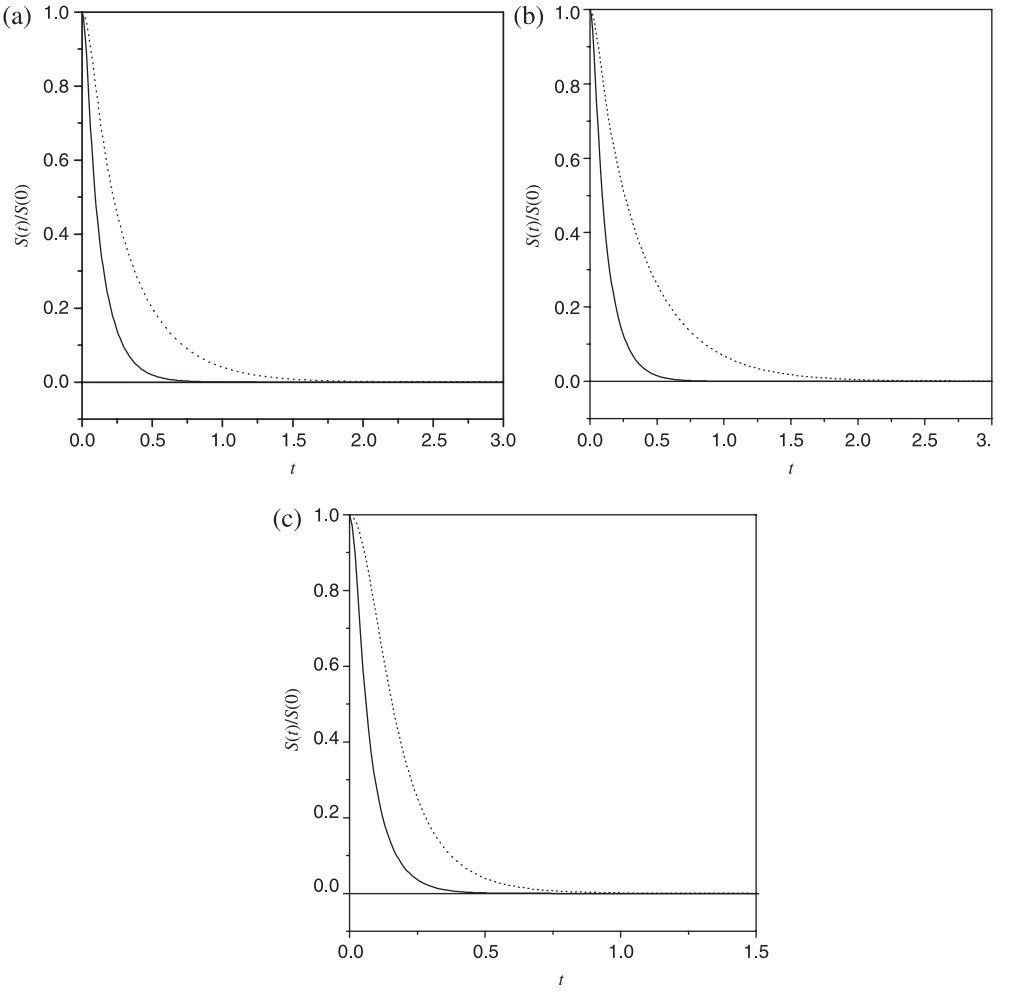

Figure 4. Normalized transverse stress auto-correlation function, $S(t)/S(0)$, *vs.* time in pico second, for (a) 1st thermodynamic state, (b) 3rd thermodynamic state, and (c) 6th thermodynamic state.

Table 6. Coefficient of shear viscosity, in centipoise, of expanded Rb for six thermodynamic states. η_{LJ} and η_{LM} represent results obtained using LJ and LM potential, respectively. η_{MD} and η_{expt} are simulation and experimental results.

State	η_{LJ}	η_{LM}	η_{MD}	η_{expt}
1	0.374	0.675	0.607	0.476
2	0.354	0.564	0.528	0.433
3	0.144	0.170	0.107	0.136
4	0.107	0.114	0.115	0.112
5	0.090	0.133	0.102	0.0996
6	0.051	0.0684	0.0774	0.0870

that the VACF of the metal and that of corresponding to the LJ potential are very similar near the critical point, which is in contrast to the behavior near the melting point. In the case of stress auto-correlation function it is found that this correlation function decays much faster in the case of harder potential than in the case of the LM for all the thermodynamic states. However, for the calculation of shear viscosity, this faster decay is somewhat compensated by larger values of shear modulus. Effect of shape of the potential on self-diffusion and shear viscosity is found to decrease as one moves toward the critical point from near the triple point. However, collective properties are found to be more sensitive to the detail of the potential than the single particle motion even near the critical point. It is also noted that three particle correlations are more important in the case of LMs than in LJ fluids with harder potential.

Acknowledgments

The authors are thankful to Professor K.N. Pathak, Panjab University, Chandigarh, for the useful discussion regarding the work, and also thank University Grants Commission (UGC) for providing the financial assistance in the form of minor research project. KT acknowledges the facilities provided as an associate member of Abdus Salam International Center for Theoretical Physics, Trieste, Italy where part of this work was done.

References

[1] J.P. Hansen, I.R. McDonald. *Theory of Simple Liquids*, Academic Press, London (1986).
[2] I. Ebbsjo, T. Kinell, I. Waller. *J. Phys. C*, **13**, 1865 (1980).
[3] M. Canales, J.A. Padro. *Phys. Rev. E*, **56**, 1759 (1997).
[4] M. Canales, J.A. Padro. *Phys. Rev. E*, **60**, 551 (1999).
[5] C. Pilgrim, R. Winter, F. Hensel, C. Morkel, W. Glaser. In *Recent Developments in Physics of Fluids*, W.S. Howells, A.K. Soper (Eds), p. F181, Hilger, Bristol (1992).
[6] G. Kahl, S. Kambayashi. *J. Phys.: Condens. Matter*, **6**, 10897 (1994).
[7] Saroj K. Sharma, K. Tankeshwar. *J. Phys.: Condens. Matter*, **8**, 10839 (1996); *Ibid*., bf, **9**, 6185 (1997).
[8] K. Tankeshwar, B. Singla, K.N. Pathak. *J. Phys.: Condens. Matter*, **3**, 3173 (1991).
[9] N.H. March, M.P. Tosi. *Introduction to Liquid State Physics*, World Scientific, Singapore (2002)
[10] S. Ranganathan, K.N. Pathak. *J. Phys.: Condens. Matter*, **6**, 1309 (1994).
[11] Raman Sharma, K. Tankeshwar. *Phys. Chem. Liq*., **32**, 225 (1996); *J. Phys.: Condens. Matter*, **9**, 6191 (1997).
[12] Rajneesh, K. Sharma, K. Tankeshwar, K.N. Pathak. *J. Phys. C: Condens. Matter*, **7**, 537 (1995).
[13] J.P. Boon, S. Yip. *Molecular Hydrodynamics*, McGraw-Hill, New York (1980).
[14] H. Mori. *Prog. Theor. Phys*., **33**, 423 (1965).
[15] R. Albaki, J.F. Wax, J.L. Bretonnet. *J. Non-Crys. Solids*, **312–314**, 153 (2002).
[16] R. Bansal, K.N. Pathak. *Phys. Rev*., **A 9**, 2773 (1974).
[17] K. Tankeshwar, K.N. Pathak, S. Ranganthan. *J. Phys. C: Solid State Phys*., 21, 3607 (1988).
[18] S. Sung, D. Chandler. *J. Chem. Phys*., **56**, 498 (1972).
[19] J.G. Kirkwood. *J. Chem. Phys*., **3**, 300 (1935).
[20] R. Ohse. *Handbook of Thermodynamics and Transport Properties of Alkali Metals*, Blackwell Scientific Publication, Oxford (1985).